City Research Online

City, University of London Institutional Repository

This is the accepted version of the paper.

This version of the publication may differ from the final published version.

Assessment of sub-Nyquist deterministic and random data sampling techniques for operational modal analysis

Kyriaki GKOKTSI [1], Agathoklis GIARALIS [2]

[1] Dpt Civil Engineering (City, University of London)
Northampton Square, EC1V 0HB - London (UK) Kyriaki.Gkoktsi.1@city.ac.uk
[2] Dpt Civil Engineering (City, University of London)
Northampton Square, EC1V 0HB - London (UK) Agathoklis.Giaralis.1@city.ac.uk

Key words: multi-coset sampling, sub-Nyquist sampling, compressive sensing, power spectrum estimation, operational modal analysis, signal sparsity.

Abstract

This paper assesses numerically the potential of two different spectral estimation approaches supporting non-uniform in time data sampling at sub-Nyquist average rates (i.e., below the Nyquist frequency) to reduce data transmission payloads in wireless sensor networks (WSNs) for operational modal analysis (OMA) of civil engineering structures. This consideration relaxes transmission bandwidth constraints in WSNs and prolongs sensor battery life since wireless transmission is the most energy-hungry on-sensor operation. Both the approaches assume acquisition of sub-Nyquist structural response acceleration measurements and transmission to a base station without on-sensor processing. The response acceleration power spectral density matrix is estimated directly from the sub-Nyquist measurements and structural mode shapes are extracted using the frequency domain decomposition algorithm. The first approach relies on the compressive sensing (CS) theory to treat sub-Nyquist randomly sampled data assuming that the acceleration signals are sparse/compressible in the frequency domain (i.e., have a small number of Fourier coefficients

with significant magnitude). The second approach is based on a power spectrum blind sampling (PSBS) technique considering periodic deterministic sub-Nyquist "multi-coset" sampling and treating the acceleration signals as wide-sense stationary stochastic processes without posing any sparsity conditions. The modal assurance criterion (MAC) is adopted to quantify the quality of mode shapes derived by the two approaches at different sub-Nyquist compression rates (CRs) using computer-generated signals of different sparsity and field-recorded stationary data pertaining to an overpass in Zurich, Switzerland. It is shown that for a given CR, the performance of the CS-based approach is detrimentally affected by signal sparsity, while the PSBS-based approach achieves MAC>0.96 independently of signal sparsity for CRs as low as 11% the Nyquist rate. It is concluded that the PSBS-based approach reduces effectively data transmission requirements in WSNs for OMA, without being limited by signal sparsity and without requiring a priori assumptions or knowledge of signal sparsity.

1 INTRODUCTION

The potential of using wireless sensor networks (WSNs) to facilitate field implementations for operational modal analysis (OMA)[1,2] of civil engineering structures has been widely recognized in the past two decades[3-6]. In particular, WSNs enable cable-free acquisition and transmission of response acceleration signals from linear vibrating structures excited by broadband ambient dynamic loads. These signals are processed using OMA algorithms to extract the structural dynamic properties (e.g., modal shapes and natural frequencies) which are further used for condition assessment, design verification, and health monitoring purposes[1,2]. In this context, WSNs reduce the up-front cost of OMA, compared to arrays of wired sensors, while they allow for less obtrusive and more rapid sensor deployment, especially in large-scale and/or geometrically complex civil engineering structures[3,4].

Nevertheless, typical wireless sensors undertaking conventional uniform-in-time signal sampling at (at least) the Nyquist rate require regular battery replacement which increase the

2

maintenance cost of WSNs in long-term OMA deployments. The frequency of replacing batteries ranges within few weeks to few months depending on various factors such as the sampling frequency, the duration of each monitoring interval, and the on-sensor data post-processing aiming for data compression[3-8]. The latter consideration reduces data transmission payloads in order to (i) prolong battery life, since wireless transmission is the most power consuming operation in a wireless sensor, and (ii) ensure the reliability of the monitoring system, since the amount of data that can be transmitted within a WSN is subjected to bandwidth limitations[3,4].

To this end, it has been recently recognized that OMA relying on non-uniform in time data sampling/acquisition techniques[9-14] at sub-Nyquist rates (i.e., average sampling rates below an assumed application-dependent Nyquist rate) is a viable alternative to off-line data compression in reducing data transmission payloads. These techniques involve simultaneous signal acquisition and compression at the sensor front-end. Therefore, requirements for on-sensor data storage are relaxed while local on-board data processing before wireless transmission is significantly reduced, or even by-passed. In this regard, most of measurement post-processing and the associated computational burden is transferred from the sensors to the server[15].

In this setting, this paper assesses the potential of two recent alternative spectral estimation approaches relying on different non-uniform in time sub-Nyquist sampling schemes to extract the mode shapes and associated natural frequencies of structures vibrating under operational ambient loading. Figure 1 juxtaposes the steps involved in each of the two approaches. Both the considered approaches involve the application of the standard frequency domain decomposition (FDD) algorithm[2] for OMA to the response acceleration power spectral density (PSD) matrix pertaining to the sensors location. Further, in both approaches, the PSD matrix is estimated directly from the compressed measurements (i.e., response acceleration data sampled

at average rates well below the Nyquist) without retrieving the traces of the acquired signals in time domain. However, PSD matrix estimation is accomplished by making significantly different assumptions for the attributes of the acquired signals and treating the compressive measurements in a completely different manner.
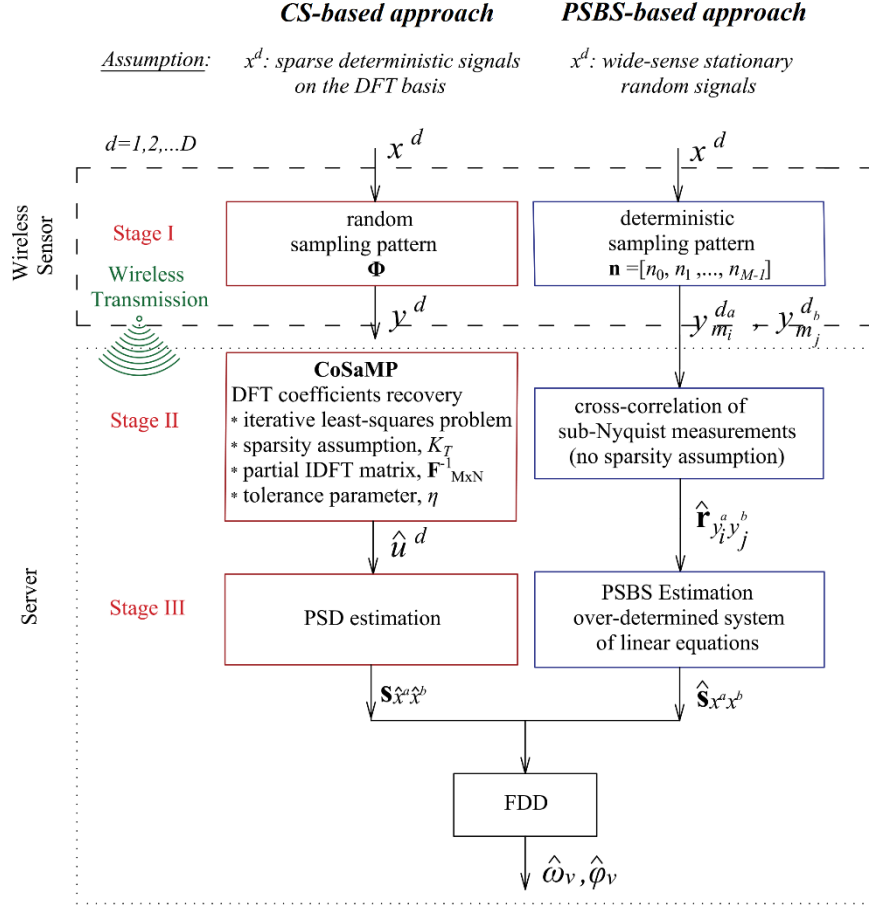

Figure 1: Flowcharts of the two different sub-Nyquist sampling and spectral estimation approaches under comparison for frequency domain OMA.

Specifically, the approach proposed by *O'Connor et al.*[9,10], delineated in the left flowchart of Figure 1, is based on the theory of compressive sensing (CS)[16-18]. It assumes that structural response acceleration signals are "sparse" on a *pre-defined* discrete Fourier transform (DFT) basis. That is, they have a relatively small, K, number of DFT coefficients with magnitude higher than an arbitrarily specified low threshold; by definition, if this threshold is set equal to zero then the signals are termed K-sparse, otherwise they are termed K-compressible[19]. Relying on this signal sparsity assumption, the considered CS-based approach uses a popular algorithm

for sparse signal recovery[19] to estimate the DFT coefficients of the response acceleration signals by acquiring $M>K$ random non-uniform in time measurements (CS-based sampling), while the standard periodogram[20] is used for the PSD matrix estimation. Notably, *O'Connor et al.*[9] achieved accurate mode shape estimation as well as appreciable savings in energy consumption via the above approach using a WSN of five sensor nodes customized for CS-based sampling to monitor an overpass in MI, USA. The sensors operated at up to 80% slower average rate compared to a concurrently operating network of conventional wireless sensors sampling uniformly in time at twice the assumed Nyquist rate. Given its successful field implementation, the approach of *O'Connor et al.*[9] is herein treated, among other approaches[11-13], as a paradigm of CS-based OMA using low-rate randomly sampled measurements with no on-sensor processing.

Importantly, in the above CS-based approach, as in all CS-based approaches for OMA[9-13] and, more generally, for structural health monitoring[8,21-24], the *minimum* average random sampling rate for which quality signal recovery can be achieved *depends strongly on and is limited by* the actual sparsity/compressibility of the monitored response acceleration signals on a pre-specified/assumed basis or frame[25,26]. At the same time, discrete-time versions of such signals, as recorded in the field, may not be significantly sparse on a DFT basis[8,9,23] partly due to unknown environmental excitation[23] and partly due to spectral leakage[27,28] associated with the fact that the assumed grid of the DFT frequencies may not coincide with the (unknown) resonant structural natural frequencies.

Outlined in the right flowchart of Figure 1, the second approach considered in this work was recently developed by the authors[14] to achieve frequency domain OMA using sub-Nyquist response acceleration measurements without imposing any signal sparsity conditions. In particular, the method treats signals as realizations of an underlying wide-sense stationary random process and estimates second-order statistics (i.e., the covariance matrix or,

equivalently, the PSD matrix) through a power spectrum blind sampling (PSBS) step assuming a deterministic periodic non-uniform-in-time sampling scheme known as multi-coset sampling[29-32].

From a practical viewpoint, it is emphasized that, contrary to the signal sparsity assumption made by the CS-based approach, the stationarity signal assumption of the PSBS-based approach does not limit the applicability of the method for OMA as the same assumption is made by the FDD algorithm[1,2]. However, it is recognized that the PSBS-based approach cannot retrieve, by default, the time-histories of response acceleration signals. It, thus, can only be applicable to structural health monitoring applications utilizing second-order random signal statistics, which is the case of frequency domain-based OMA pursued in this work. In this regard, the main contribution of this paper is the quantitative numerical assessment of the effect of the signal sparsity assumption required by the CS-based approach to the achieved data compression level for accurate modal properties estimation. This is accomplished by furnishing novel results pertaining to the application of the two different sub-Nyquist spectral estimation approaches in Figure 1 for two different case-studies. The first case study involve computer-generated response acceleration signals of a white-noise excited simply supported steel beam corrupted by additive Gaussian white noise. The second case study considers field recorded response acceleration time-histories from an overpass in Zurich, Switzerland, monitored under operational conditions[33,34]. In both case studies, performance is quantified in terms of the modal assurance criterion (MAC)[2] of mode shapes derived from a fixed number of compressed measurements. Focus is given on gauging the sparsity requirements of the CS-based approach and on numerically verifying that the accuracy of the PSBS-based approach is insensitive to signal sparsity. Emphasis is also placed on quantifying the level of signal compression that can be reached by the different compressive sampling schemes utilized in the two approaches, while achieving accurate mode shapes with MAC>0.9. From the methodological viewpoint, it

is noted that the undertaken comparative numerical study is facilitated by the fact that both approaches utilize the same frequency-domain OMA algorithm (FDD). Therefore, any differences to the quality of mode shapes achieved by the competing methods can be attributed to the different low-rate sampling schemes, and to the limitations posed by the associated post-processing methods applied to the compressed measurements. Furthermore, the fairness of the comparison in relation to up-front and/or operational monitoring costs is safeguarded by the fact that neither of the approaches consider on-sensor data processing before transmission, while no prior knowledge on the properties (i.e., the sparsity) of the acquired signals is assumed available. The latter would theoretically benefit the CS-based approach but would require either the use of an additional complementary network of wired sensors[11] incurring additional monitoring costs, or increased energy demands due to fast (conventional) uniform-in-time sampling and heavy data post-processing on the wireless sensors[21-24]. Instead, this study assumes the availability of sensors that acquire and transmit signals directly in the compressed domain supporting low-power WNSs[9].

The remainder of the paper is organized as follows. Section 2 reviews briefly the adopted CS-based approach[9,10] shown in the left flow-chart of Figure 1. Section 3 outlines the theoretical background of the PSBS-based spectral estimation approach[14] shown in the right flow-chart of Figure 1. Sections 4 and 5 furnish comparative numerical results and discussion pertaining to computer simulated and field recorded response acceleration measurements, respectively. Finally, Section 6 summarizes concluding remarks.

2 COMPRESSIVE SENSING (CS)-BASED APPROACH

Consider a deterministic N-long discrete-time (response acceleration) signal $x[n] \in \mathbb{R}^N$ being K-sparse/compressible on the DFT basis. The signal is expressed as

$$x[n] = \mathbf{F}_{N \times N}^{-1}\, u[n], \tag{1}$$

where $\mathbf{F}_{N \times N}^{-1} \in \mathbb{C}^{N \times N}$ is the inverse discrete Fourier transform (IDFT) matrix, and $u[n] \in \mathbb{C}^{N}$ is the vector collecting the DFT coefficients of the considered signal having K entries with significant magnitude, where $K \ll N$. CS theory[16-18] asserts that the information contained in this K-sparse signal $x[n]$ can be retrieved in a robust manner from M non-uniform random measurements $y[m] \in \mathbb{R}^{M}$, where $K < M \ll N$, and M/N is defined as the *compression ratio* (*CR*). This is achieved by employing a measurement matrix $\mathbf{\Phi} \in \mathbb{C}^{M \times N}$ during sampling that satisfies the so-called restricted isometry property (RIP)[35], associated with the orthonormality level of the columns of $\mathbf{\Phi}$. In this work, a $\mathbf{\Phi}$ matrix populated with incoherent measurements of zero-one entries that randomly selects M rows from the standard orthonormal IDFT matrix in Eq. (1) is assumed, which defines the "partial" Fourier matrix $\mathbf{F}_{M \times N}^{-1} \in \mathbb{C}^{M \times N}$. To this end, the compressed signal (i.e., vector collecting the M compressed measurements) $y[m]$ is given by

$$y[m] = \mathbf{\Phi} \mathbf{F}_{N \times N}^{-1} u[n] + \mathbf{e} = \mathbf{F}_{M \times N}^{-1} u[n] + \mathbf{e}, \qquad (2)$$

where $\mathbf{e}$ is a vector representing measurement errors at the sensor. It is important to note that the error term in Eq.(2) is added to the compressed measurements and does not influence the sparsity level K of the signal $x[n]$. Such errors are treated by all standard CS sparse recovery algorithms, as the one discussed below, by solving the so-called "noisy" sparse recovery problem. However, in the numerical work of Section 4, noise is added to the signal $x[n]$ in Eq.(1). Such additive noise *does* influence the sparsity of the signal and cannot be rectified during CS sparse recovery[25].

Next, the dominant K DFT coefficients of $x[n]$ are recovered from the compressed measurements $y[m]$ in Eq. (2) by using the iterative matching pursuit algorithm CoSaMP[19]. This particular algorithm was used by *O'Connor et al.*[9,10] for sparse recovery out of numerous alternatives[36] and is also adopted in the ensuing numerical work. CoSaMP takes as input the compressed observation vector $y[m]$ in Eq. (2), the partial IDFT measurement matrix $\mathbf{F}_{M \times N}^{-1}$, a

target sparsity level K_T, which should be less than $M/3$, (i.e., $K_T<M/3$), and a tolerance parameter η. It returns a K_T-sparse estimate $\hat{u}[n]$ of the K-sparse DFT spectrum $u[n]$ that satisfies the condition

$$\left\| u[n]-\hat{u}[n] \right\|_{\ell_2} \le C \cdot \max\left\{ \eta, \frac{1}{\sqrt{K_T}}\left\| u[n]-u_{K_T/2}[n] \right\|_{\ell_1} + \left\|\mathbf{e}\right\|_{\ell_2} \right\}, \qquad (3)$$

where $u_{K_T/2}[n]$ is the optimal $K_T/2$-sparse approximation of $u[n]$, C is a constant, and $\left\|\mathbf{a}\right\|_{\ell_p}$ is the ℓ_p norm of a. In each iteration, CoSaMP captures part of the energy of the target signal by solving a least-squares problem involving the pseudoinverse of the matrix $\mathbf{F}^{-1}_{M\times N}$ in Eq. (2)[19]. The extracted energy is subtracted from the target signal and in the next iteration the residual signal becomes the target signal. This iterative process continues until any of the following three stoppage criteria is met: (i) the relative residual signal energy between two iterations is less than the tolerance η, or (ii) the total residual energy in the last iteration is smaller than η, or (iii) a predefined maximum number of iterations is reached.

Following the OMA approach in *O'Connor et al.*[9,10] illustrated in Figure 1 (left flowchart), the above CS-based data sampling and sparse recovery steps are applied to an array of D identical CS-based sensors. Each sensor d, $d=1,2,…,D$, compressively senses structural response acceleration signals $x^d[n]$ at stage I, and wirelessly transmit the compressed measurements $y^d[n]$ to a base station (server). The CoSaMP algorithm is then employed at stage II to derive D estimates of the K_T-sparse DFT coefficients, $\hat{u}^d[n]$, on the uniform Nyquist grid. These coefficients can be used in a straightforward manner to obtain an estimate of the PSD matrix in stage III using any standard spectral estimation technique assuming uniform Nyquist sampling in time domain[20]. As a final step, the standard FDD algorithm is applied to the PSD matrix obtained by the above CS-based approach to derive structural modal properties (natural frequencies and mode shapes).

It is important to note that the two critical parameters for robust and accurate structural modes shape estimation (in the context of the above CS-based approach for OMA) are: (i) the number of compressed measurements M, which should be of the order $M \sim O(K \cdot \log(N))$ for reasonably accurate sparse approximation of the DFT coefficients of field recorded response acceleration signals, as reported by *O'Connor et al.* [9,10] ; and (ii) the target sparsity level K_T assumed in the sparse signal recovery step, which is associated with a trade-off between reconstruction accuracy and computation complexity. Choosing a relatively large value of K_T ($>>K$) leads to unnecessarily high computational cost, as the latter is bounded by

$$O\left(K_T \cdot M \cdot N + log\left(\|x\|_{\ell_2}/\eta\right) \cdot K_T \cdot M\right)$$ [19]. On the antipode, a relatively small value of K_T ($<<K$)

may lead to poor approximation of the Fourier coefficients of the vibration measurements and, therefore, to low quality mode shape estimation. In practice, a range of different K_T values should be tested (off-line) to strike a good balance between accuracy and computational complexity. It thus becomes obvious that both M and K_T parameters depend on the signal sparsity level K which is adversely affected by broadband environmental noise while it is unknown, unless *a priori* knowledge becomes available through conventional uniform-in-time sampling and signal processing[11,23-25]; a scenario that is not addressed in this paper. In the next section, an alternative spectral estimation approach relying on low-rate (sub-Nyquist) measurements is reviewed which does not depend on signal sparsity.

3 POWER SPECTRUM BLIND SAMPLING (PSBS)-BASED APPROACH

Consider now the sub-Nyquist spectral estimation approach shown in the right flowchart of Figure 1. Let $x(t)$ be a continuous in time t real-valued wide-sense stationary random signal (or stochastic process) characterized in the frequency domain by the power spectrum $P_x(\omega)$ band-limited to $2\pi/T$. It is desired to sample $x(t)$ at a rate lower than the Nyquist sampling rate $1/T$ (in Hz), and still be able to obtain a useful estimate of the power spectrum $P_x(\omega)$. To this aim, the multi-coset sampling is adopted[29,30] at stage I, according to which the uniform grid of

Nyquist sampled measurements $x[n] \in \mathbb{R}^N$, is first divided into P blocks of $\bar{N}$ consecutive samples, where $\bar{N}=N/P$. From each block $p=\{1,2,\ldots P\}$, a number of $\bar{M}$ samples ($\bar{M} < \bar{N}$) is selected at a deterministically pre-specified position which remains the same for all blocks. The acquired number of samples further defines the associated *CR* given as $\bar{M}/\bar{N}$. In this manner, the multi-coset sampling strategy yields non-uniform-in-time deterministic $\bar{N}$-periodic samples; this is very different from the CS-based aperiodic random sampling briefly reviewed in the previous section.

From a practical viewpoint, note that, as in the case of CS-based random sampling, there are currently no commercially available sensors implementing sub-Nyquist multi-coset sampling for structural health monitoring purposes. However, despite practical implementation difficulties, efficient prototypes of compressive multi-coset samplers have been recently developed [31,37].

For illustration, Figure 2 shows a discrete-time model of an ideal multi-coset sampler[30], in which the *p*-th block of signal $x[n]$ enters $\bar{M}$ channels and at each *m* channel ($m=0,1,\ldots, \bar{M}-1$), the input signal is convolved with an $\bar{N}$-length sequence $c_m[n]$ and down-sampled by $\bar{N}$.
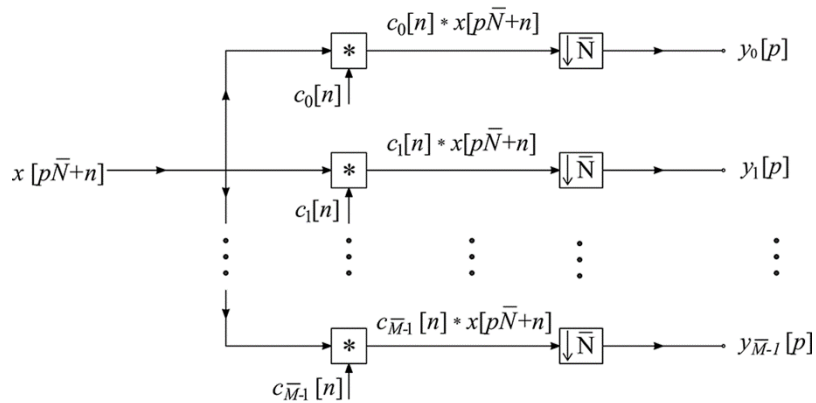

Figure 2: Discrete-time model of the considered multi-coset sampling device[30]

The selection of $\bar{M}$ samples within each $\bar{N}$-length block is given by the sampling pattern $\mathbf{n} = [n_0 \quad n_1 \quad \cdots \quad n_{\bar{M}-1}]^T$ which defines the difference set $S = \left\{ \left| n_{mi} - n_{mj} \right|, n_{mi}, n_{mj} \in \mathbf{n} \right\}$. The

latter arises naturally in the computation of the auto/cross correlation sequences of discrete time signals, required for the blind recovery of the unknown power spectra of non-sparse signals pertaining to any structure. Further, the multi-coset sampling pattern is governed by the filter coefficients $c_m[n] = 1$ for $n = -n_m$, and $c_m[n] = 0$ for $n \neq -n_m$, where there is no repetition in n_m, i.e., $n_{m_i} \neq n_{m_j}, \forall\, m_i \neq m_j$. The output of the m-th channel of the considered sampling device is given by the convolution operation $y_m[p] = \sum_{n=0}^{\bar{N}-1} c_m[-n]\, x[p\bar{N} + n]$ as indicated in Figure 2.

Importantly, the encoded information carried within the output signal $y_m[p]$ ($m = 0,1,\ldots,$ $\bar{M}-1$) can be retrieved from the cross-correlation estimates among all M channels of the adopted multi-coset sampler collectively. Thus, the difference set, S, is utilized to estimate the correlation sequence of the signal $x[n]$ at almost all lags within a given range, i.e. [-L, L], outside which the correlation estimate takes on negligible values. In practice, the latter will hold for some L depending on the level of damping of the monitored structural system.

Consider, next, an array of D identical multi-coset samplers with $\bar{M}$ channels each, the cross-correlation function

$$r_{y_i^a, y_j^b}[k] = \mathrm{E}_\mathrm{y}\left\{ y_{m_i}^{d_a}[l]\, y_{m_j}^{d_b}[l-k] \right\}, \tag{4}$$

of the output signals $y_{m_i}^{d_a}[l]$, $y_{m_j}^{d_b}[l]$ can be computed for all m_i, $m_j = 0,1,\ldots,\bar{M}-1$ channels and d_a, d_b=1, 2,…, D devices (see also stage II in the right flowchart of Figure 1). In the above equation, $\mathrm{E}_\mathrm{a}\{\cdot\}$ is the mathematical expectation operator with respect to a. Further, the following relation holds[14]

$$\mathbf{r}_{\mathrm{y}^a\mathrm{y}^b} = \mathbf{R}_\mathrm{c}\mathbf{r}_{x^a x^b}, \tag{5}$$

where $\mathbf{r}_{y^a y^b} \in \mathbb{R}^{\bar{M}^2(2L+1)\times D}$ is a matrix collecting the cross-correlation sequences in Eq. (4)

12

computed within the range (support) $-L \leq k \leq L$. Similarly, $\mathbf{r}_{x^a x^b} \in \mathbb{R}^{\bar{N}(2L+1) \times D}$ is a matrix

collecting the input cross-correlation sequences, $r_{x^a x^b}[k] = \mathrm{E}_x\left\{ x^{d_a}[n]\, x^{d_b}[n-k] \right\}$ computed for

all d_a and d_b devices in the above range, and $\mathbf{R}_c \in \mathbb{R}^{\bar{M}^2(2L+1) \times \bar{N}(2L+1)}$ is a sparse pattern correlation

matrix populated with the cross-correlations[30] $r_{c_i,c_j}[\tau] = \sum_{n=1-N}^{0} c_{m_i}[n] c_{m_j}[n-\tau]$. Note that Eq.

(5) defines an overdetermined system of linear equations which can be solved for $\mathbf{r}_{y^a y^b}$ without

any sparsity assumptions, provided that $\mathbf{R}_c$ is full column rank. The latter is satisfied for

$\bar{M}^2 \geq \bar{N}$.

The unbiased estimator of the output cross-correlation function in Eq. (4) is then adopted,

$$\hat{r}_{y_i^a, y_j^b}[p] = \frac{1}{P-|p|} \sum_{l=\max\{0,p\}}^{P-1+\min\{0,p\}} y_{m_i}^{d_a}[l] y_{m_j}^{d_b}[l-p], \tag{6}$$

in which P is the number of measurements that should be greater than L ($P \geq L$) for perfect

power spectral recovery. Equation (6) is further used at stage III together with the DFT matrix,

$\mathbf{F}_{(2L+1)\bar{N}} \in \mathbb{C}^{\bar{N}(2L+1) \times \bar{N}(2L+1)}$, to obtain an estimate of the input cross-spectra $\mathbf{s}_{x^a x^b}$ at the discrete

frequencies $\omega = [0, 2\pi/(2L+1)\bar{N}, \dots, 2\pi((2L+1)\bar{N}-1)/(2L+1)\bar{N}]$ [32]

$$\hat{\mathbf{s}}_{x^a x^b} = \mathbf{F}_{(2L+1)\bar{N}} \left(\mathbf{R}_c^{\mathrm{T}} \mathbf{W}^{-1} \mathbf{R}_c \right)^{-1} \mathbf{R}_c^{\mathrm{T}} \mathbf{W}^{-1} \hat{\mathbf{r}}_{y^a y^b}. \tag{7}$$

In the above equation, $\mathbf{W}$ is a weighting matrix, and the superscript "−1" denotes matrix

inversion. The solution of Eq. (7) relies on the weighted least square criterion

$$\hat{\mathbf{r}}_{x^a x^b} = \arg\min_{\mathbf{r}_{x^a x^b}} \left\| \hat{\mathbf{r}}_{y^a y^b} - \mathbf{R}_c \mathbf{r}_{x^a x^b} \right\|_{\mathbf{W}}^2, . \tag{8}$$

in which the weighted version of the Euclidean norm is given by $\|\mathrm{a}\|_{\mathbf{W}}^2 = \mathrm{a}^{\mathrm{T}} \mathbf{W} \mathrm{a}$. Note that

the cross-spectra in Eq. (7) are efficiently computed directly from the output cross-correlation

estimator $\hat{\mathbf{r}}_{y^a y^b}$, obtained from the compressed measurements of the D sampling devices, by exploiting the sparse structure of $\mathbf{R}_c$. As a final step, the PSD matrix in Eq. (7) is treated by the FDD algorithm to extract mode shapes and natural frequencies[14].

The critical parameters of the above briefly reviewed sub-Nyquist multi-coset sampling PSBS approach for OMA are the number of cosets (or channels in Figure 2), $\bar{M}$, and the value of down-sampling $\bar{N}$, subject to the two constraints $\bar{M} < \bar{N}$ and $\bar{M}^2 \geq \bar{N}$. These constraints are not very restrictive and will allow for spanning a good range of different *CRs* expressed by the ratio $\bar{M} / \bar{N}$. Therefore, once the values of $\bar{M}$ and $\bar{N}$ are fixed, the weighting matrix $\mathbf{W}$ in Eq.(7) and the sampling pattern $\mathbf{n} = [n_0 \quad n_1 \quad \cdots \quad n_{\bar{M}-1}]^T$ is determined by solving a constrained least-squares optimization problem. Some further mathematical details on this issue can be found in *Tausiesakul and Gonzalez-Prelcic*[32].

4 NUMERICAL ASSESSMENT FOR SIMULATED SIGNALS OF DIFFERENT SPARSITY LEVEL

4.1 Computer-simulated acceleration response signals

In this section, the effectiveness of the two sub-Nyquist spectral estimation approaches in Figure 1 for OMA is assessed by considering simulated noisy structural acceleration response signals obtained from the finite element model (FEM) in Figure 3. The modelled structure is an IPE300-profiled simply supported steel beam with 5m length and flexural rigidity EI= $16.78 \cdot 10^3$ kNm^2, which is assumed to be instrumented with a dense array of D=15 sensors measuring vertical accelerations along its length. The assumed sensor locations are shown with white cross marks in Figure 3.
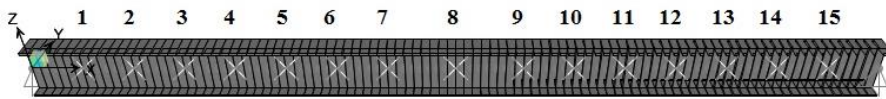

Figure 3: Finite element model of a simply supported steel beam instrumented with 15 sampling devices measuring acceleration response signals along the z-axis.

The adopted FEM is base-excited by a band-limited low-amplitude Gaussian white noise force, observing a sufficiently flat spectrum in the frequency range up to 1000Hz. The considered excitation is applied along the gravitational axis of the beam, having a duration of 4s and a time discretization step equal to 0.0005s.

Next, linear response history analysis is conducted, assuming a critical damping ratio of 1% for all modes of vibration which is a reasonable value for a bare steel structure[38]. Vertical response acceleration time-series are recorded at the 15 locations shown in Figure 3, with Nyquist sampling rate at 2000Hz (i.e., 8000 "Nyquist samples" per signal). The acquired acceleration responses are contaminated with additive Gaussian white noise expressed by the signal-to-noise ratio $SNR = 10 \cdot \log_{10}\left(\sigma_x^2 / \sigma_e^2\right)$, where σ_x^2 is the variance of the response acceleration signal and σ_e^2 is the noise variance. Two limiting SNR values are considered to simulate response datasets associated with different sparsity levels: (i) a practically a noiseless case with $SNR = 10^{20}$dB (i.e., the noise variance σ_e^2 takes on a very small value close to zero), yielding "high-sparse" signals on the DFT basis; and (ii) a noisy case with $SNR = 10$dB (i.e., the noise variance σ_e^2 equals the 10% of the signal variance σ_x^2) yielding "low-sparse" signals. For illustration, Figure 4 plots a low-sparse acceleration response signal in time (left panel), its single-sided magnitude Fourier spectrum normalized to its peak value (middle panel), as well as the normalized magnitude Fourier coefficients sorted in descending order (right panel).
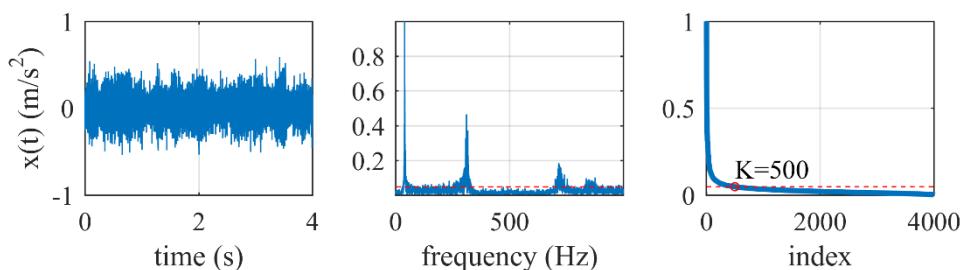

Figure 4: Typical noisy acceleration response signal with SNR=10dB; (left panel): time history; (middle panel): normalized single-sided Fourier spectrum magnitude; (right panel): Normalized magnitude Fourier coefficients in descending order. The red broken line signifies an arbitrary threshold at normalized Fourier magnitude of 0.05.

From the middle panel in Figure 4, it is readily observed that three dominant harmonics are included in the signal on top of broadband noise, corresponding to the three first flexural mode shapes of the beam. By inspection, a threshold is set in the right panel of Figure 4 (red broken line) to indicate that the significant signal energy is captured from about 500 Fourier coefficients and thus, a sparsity level of approximately K=500 may be assumed for the considered noisy signals (see also *O'Connor et al.*[9,10]). It is emphasized that this threshold can only be heuristically defined and is related to the concept of approximating a K-sparse signal by a K-compressible signal provided that the coefficients of the latter on a given basis function decay rapidly when sorted by magnitude. It is also important to clarify that the considered CS-based spectral estimation approach assumes no prior knowledge on the actual sparsity level K, but this is only reported here to facilitate the interpretation of the comparative results presented in sub-section 4.3.

4.2 Sub-Nyquist sampling and power spectral estimation

The acceleration response signals generated as detailed above are next compressively sampled at two different *CRs* of approximately 31% and 11% (i.e., 69% and 89% fewer samples compared to the Nyquist samples) using the random CS-based sampling scheme of section 2 and the deterministic multi-coset sampling scheme of section 3. The adopted sampling parameters are collected in Table 1. Specifically, a *CR*= 31% is achieved by multi-coset samplers comprising $\bar{M}$ =5 channels, where each channel samples uniformly in time with a rate $\bar{N}$ =16 times slower than the Nyquist rate. The adopted sampling pattern is $\mathbf{n}$ = [0 1 2 5 8]$^\mathrm{T}$. In this respect, only M=2500 samples are acquired by each sensor out of the N=8000 Nyquist samples. This exact pair of M, N values (i.e., M=2500, N=8000) is further used to define the partial IDFT matrix $\mathbf{F}_{M \times N}^{-1} \in \mathbb{C}^{2500 \times 8000}$ in Eq. (2) for the CS-based approach. The effectiveness of the CS-based approach is assessed for various assumed (target) sparsity levels $K_T (\leq \max(M/3,K))$ in the range of [50, 500]. For the case of *CR*=11%, the pertinent parameters

16

are defined in a similar manner as above, such that the same number of compressed measurements are acquired and transmitted by each sensor node for both the CS and the multi-coset sampling schemes.

Table 1: Considered parameters for the CS-based and the PSBS-based approaches for OMA of the structure in Figure 3 for two different compression ratios.

	Compression ratio	CR	31%	11%
Common parameters for both approaches	Number of samples uniformly acquired in time	N	8000	8000
	Sub-Nyquist Sampling Rate (Assumed Nyquist sampling rate at 2000Hz)		**69%**	**89%**
	Number of Sub-Nyquist/Compressed samples	M	2500	875
CS-based approach	Target Sparsity Level	K_T	50-500	50-290
PSBS-based approach	Number of channels	$\bar{M}$	5	14
	Down-sampling	$\bar{N}$	16	128
	Sampling pattern	**n**	$[0,1,2,5,8]^T$	$[0,1,2,6,8,20,29,38,47,50,53,60,63,64]^T$

Next, power spectral density matrices collecting estimates of the auto- and cross- power spectra of the acceleration signals from the D=15 sensors are obtained using the two considered spectral estimation methods in Figure 1 as detailed in sections 2 and 3. Specifically, for the CS-based approach, the power spectral density functions are derived in three stages: (i) compressive sensing using the matrix in Eq. (2); (ii) recovery of DFT coefficients using the CoSaMP algorithm in Eq. (3) with an assumed target sparsity K_T and stopping criteria determined by tolerance $\eta=10^{-8}$ and predefined maximum number of iterations set at 50; and finally (iii) power spectrum estimation using the standard Welch's modified periodogram[20]. The latter is applied to time-domain reconstructed acceleration responses, $\hat{x}[n]$, obtained by application of the IDFT to the recovered signal coefficients, $\hat{u}[n]$, using Eq (1). To this end, the "cpsd" built-in function in MATLAB® is adopted herein, in which the reconstructed signals are divided in eight segments with 50% overlap and windowed with a Hanning function.

For illustration, the left panel in Figure 5 evaluates the recovery performance of the CoSaMP

algorithm by plotting the CS reconstruction error, $\left\|\hat{u}[n]-u[n]\right\|_{\ell_2} / \left\|u[n]\right\|_{\ell_2}$, as a function of the target sparsity, K_T, for both the examined *CRs* (i.e., 31% and 11%), at the two limiting *SNRs* values (i.e., 10^{20}dB, 10dB). For the case of *CR*=31%, smaller reconstruction errors are observed at higher K_T values, suggesting more accurate estimates as the number of recovered measurements increases. This can be visualized at the top right panels of Figure 5 for *CR*=11%, in which case the reconstruction error increases with K_T. This rather poor reconstruction performance is because an overly high compression level was assumed for which the relatively small number of sub-Nyquist measurements $y[m]$ in Eq. (2) do not retain sufficient information of the structural response signals. Adopting, for example, the heuristic value of K=500 in Figure 4 (for the low-sparse signals with *SNR*=10dB), the required M value should be of the order of $K \cdot \log(N)= 500 \cdot \log(8000) \approx 1950$; however, only M=875 sub-Nyquist samples are acquired at *CR*=11%, which are evidently too few. Along these lines, the bottom right panels of Figure 5 confirm that the assumption of higher K_T values closer to the upper bound of $M/3 \approx 290$ cannot compensate for the insufficient number of compressed measurements, yielding spurious large amplitudes in the recovered DFT coefficients that increases the reconstruction error and adversely affects the accuracy of the obtained modal estimates, which will be presented in the next sub-section. Similar conclusions have also been reported by O'Connor et al.[9,10].

Moving to the PSBS-based approach, the PSD matrix is estimated through the following three stages: (i) multi-coset sampling based on the sampling pattern in Table 1; (ii) cross-correlation estimation applied to the compressed measurements as in Eq. (6); and (iii) power spectrum estimation using Eq. (7). The recovered PSD estimates are illustrated in Figure 6 (red curve) for the two adopted *CRs* at 31% (left) and 11% (right), respectively, considering the low-sparse dataset. For comparison, Figure 6 also plots the pertinent PSD curves obtained from the standard Welch's modified periodogram at Nyquist rate (black curve), and reports the mean square error (MSE) of the two comparative PSDs. It is readily observed that more ripples are

found for lower *CRs* (left panel), which increases the MSE value. Nonetheless, the spectral peaks are well captured from the PSBS approach in both amplitude and shape even for *CR*=11%, which is essential for accurate modal identification.
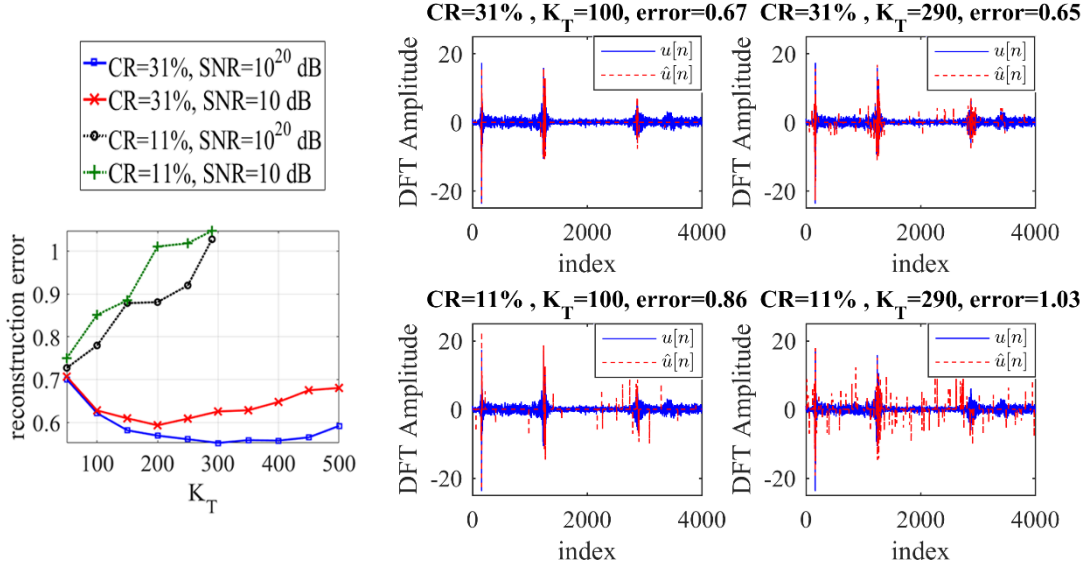

Figure 5: Signal reconstruction error of CoSaMP algorithm versus the target sparsity level K_T (left); original and reconstructed DFT coefficients at CR={31%,11%}, K_T={100, 290} for SNR=10 dB (right).
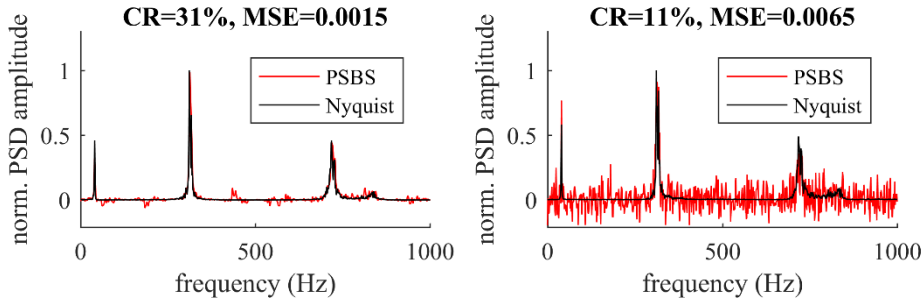

Figure 6: PSBS spectral recovery and MSE for the low-sparse response accelerations (SNR=10 dB) at CR=31% (left) and CR=11% (right).

4.3 Mode shapes estimation

The FDD algorithm is lastly applied to the PSD matrices obtained as detailed above to extract the modal properties of the beam in Figure 3. For illustration, Figure 7 presents all three excited mode shapes derived from the noisy (i.e., lower-sparsity) measurements, as extracted from the two different approaches (CS-based for K_T=290 and PSBS-based) for *CR*=31%. In Figure 8 only the first two mode shapes are shown for *CR*=11% and for *SNR*=10dB since the

third mode is not detectable at this low *CR*. For comparison, Figure 7 and 8 plot further the mode shapes obtained by application of the FDD to the conventionally (Nyquist) sampled measurements, considering the Welch periodogram[20] with the same settings as detailed in the previous sub-section. From a qualitative viewpoint, it is observed that both sub-Nyquist approaches perform well for *CR=31%* in capturing the shape and relative amplitude of the modal deflected shapes compared to the conventional approach, with the PSBS-based method being slightly more accurate. For higher signal compression at *CR=11%,* the PSBS-based method clearly outperforms the CS-based method.
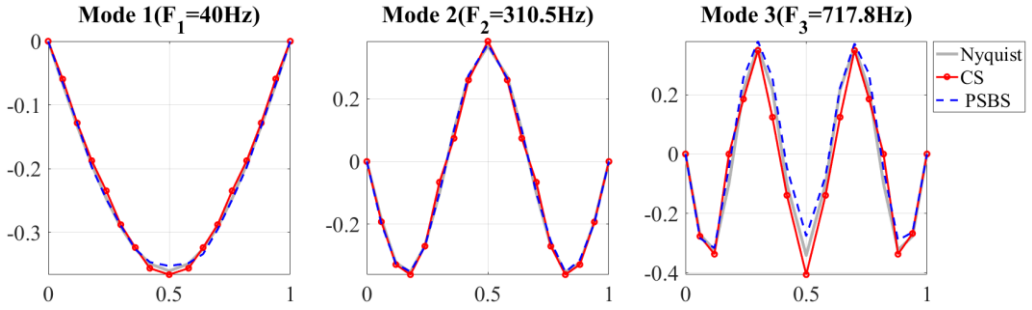

Figure 7: Mode shape estimation for CR*=31%,* SNR*=10dB (low-sparse signals) and target reconstruction sparsity K_T=290 for the CS-based approach*
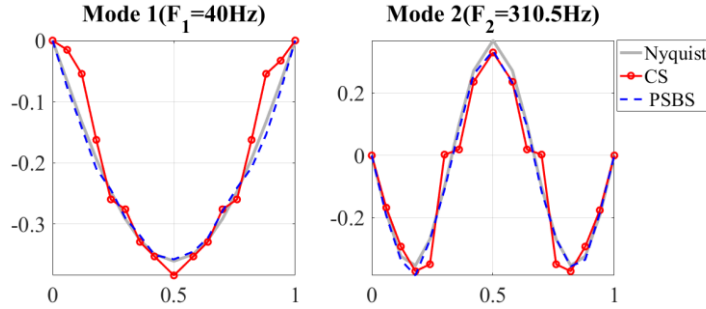

Figure 8: Mode shape estimation for CR*=11%,* SNR*=10dB (low-sparse signals) and highest possible target reconstruction sparsity K_T=290 in the CS-based approach*

To quantify the level of accuracy for the extracted mode shapes, the modal assurance criterion (MAC)[2]

$$MAC(\varphi,\hat{\varphi}) = \frac{\left|\varphi^{\mathrm{T}}\hat{\varphi}\right|^2}{\left\|\varphi\right\|_{\ell_2}^2 \left\|\hat{\varphi}\right\|_{\ell_2}^2}$$

(9)

is considered which measures the correlation between the modes shapes, $\hat{\varphi}$ and φ, estimated

by means of the FDD algorithm from compressed (sub-Nyquist) and Nyquist samples, respectively, with $\|\varphi\|_{\ell_2}$ denoting the ℓ_2 norm of φ. The normalized inner product in Eq. (9) yields a scalar value within the range of [0, 1] and values of 0.9 and higher suggests acceptable overall similarity/proximity between the $\hat{\varphi}$ and φ vectors. Figure 9 and 10 plot the computed MAC values with respect to the assumed target sparsity K_T for both the relatively high-sparse (SNR=10^{20}dB) and low-sparse (SNR=10dB) signals for CRs at 31% and 11%, respectively.
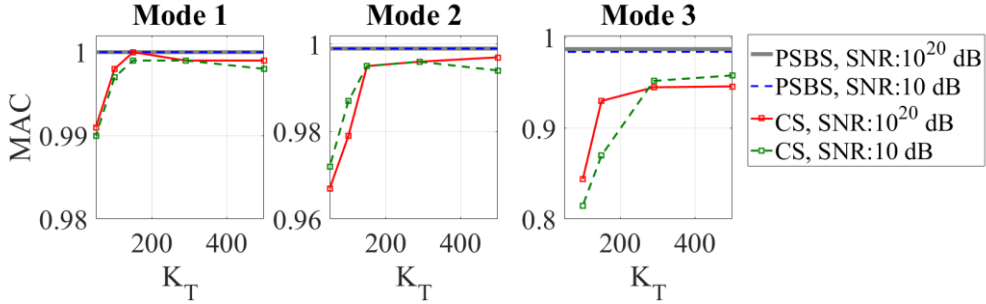

Figure 9: MAC versus reconstruction sparsity level K_T, obtained from the two considered approaches, PSBS-based and CS-based FDD, for CR= 31% and SNR={10^{20},10}dB
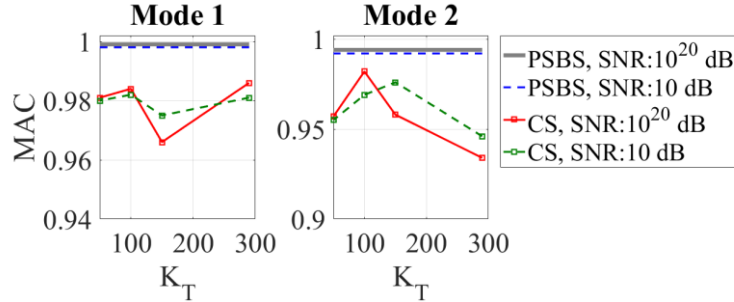

Figure 10: MAC versus reconstruction sparsity level K_T, obtained from the two considered approaches, PSBS-based and CS-based FDD, for CR= 11% and SNR={10^{20},10}dB

The above figures show that for both sparsity levels, the PSBS-based approach outperforms the CS-based approach for the same number of acquired (and wirelessly transmitted) sub-Nyquist measurements regardless of the adopted target sparsity K_T value. Specifically, the PSBS-approach can accurately retrieve the modal deflected shapes yielding MAC values close to unity. Notably, the PSBS method does not rely on sparsity assumptions, and therefore the obtained MAC values are not functions of K_T. Still, Figure 9 shows that the CS-based approach does perform quite well at least for CR=31%, though its performance depends heavily on the

assumed K_T value. Importantly, for CR=31% higher accuracy is achieved for higher K_T values (note also the decreasing trend in the reconstruction error curve in Figure 5), but this comes at the cost of higher computational demands in the signal reconstruction step. However, this is not the case for CR=11% and for the second and less excited mode shape in Figure 10, where the accuracy deteriorates yielding lower MAC values with increasing K_T. This rather unfavorable condition can be explained through Figure 5, where it is numerically shown that higher CS reconstruction errors occurs at larger K_T values for CR=11%, having a profound impact on the accuracy of the obtained CS modal results. In this case, if *a priori* knowledge of the signal sparsity was known[11,21-24], then one should normally opt to increase the average random sampling rate (i.e., obtain a larger number of measurements, M, within the same time frame). Nevertheless, the signal agnostic PSBS approach is capable to extract structural mode shapes associated with the local peaks of the spectrum even for CR=11% and signals with lower sparsity (at SNR=10dB) as long as they are not completely "buried" in noise. For instance, the right panel of Figure 6 reveals that the recovered PSBS-PSD at CR=11% and SNR=10dB exhibits attains relatively large amplitudes close to the 3rd spectral peak, which hinders the extraction of the associated vibrating mode of the beam in Figure 3.

As a final remark, it is noted that both the adopted sub-Nyquist methods yield fairly accurate natural frequency estimates in all considered cases (error is less than 1% compared to the conventional approach at Nyquist rate).

5 NUMERICAL ASSESSMENT FOR FIELD-RECORDED SIGNALS

5.1 The Bärenbohlstrasse bridge case-study and pre-processing of recorded data

Further to the previous comparison and along similar lines, the effectiveness of the two considered spectral estimation approaches of Figure 1 is herein assessed against field recorded data from an existing bridge, namely the Bärenbohlstrasse overpass in Zurich, Switzerland[33,34], vibrating under operational loading. The bridge is 30.90m long, having a deck of variable

width, while it is almost symmetric along the longitudinal direction. It consists of a solid prestressed-slab with two equal-length spans of 14.75m each. The deck is supported, via steel bearings, in all directions at mid-span and in one of the abutments. The second abutment supports the deck only in the vertical and transverse directions. The bottom face of the deck was permanently instrumented for the 12-month period of 12th July 2013 to 26th July 2014 by a network of 18 tethered sensors measuring vertical response acceleration signals at an hourly basis. Measurements were acquired at the sampling rate of 200Hz (T=0.005s) for approximately 10min per hour. A photo of the bridge and a sketch of the sensors layout is shown in Figure 11. Further details regarding the bridge, the sensors installation and data acquisition can be found in *Spiridonakos et al.*[33] and in *Chatzi and Spiridonakos*[34].
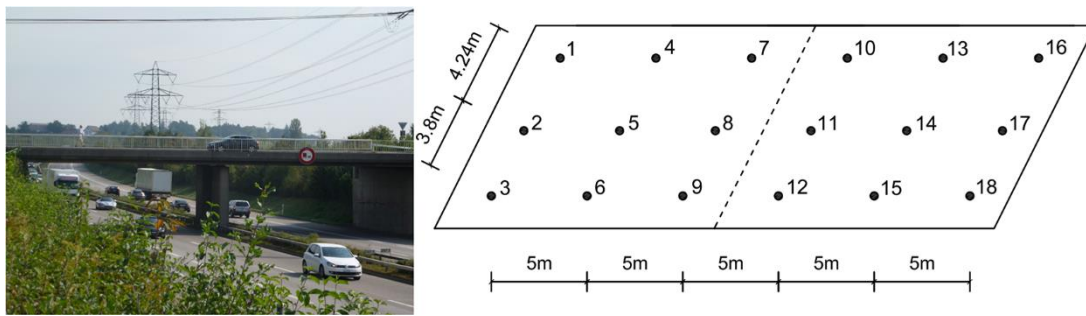

Figure 11: Bärenbohlstrasse bridge in Zurich, Switzerland (image reused from Spiridonakos et al [33]) (left) and layout of the 18 sensors recording vertical acceleration responses under ambient excitation (right).

In this study, a dataset of 18 vertical acceleration response signals is used, recorded on 19/06/2014 between 15:08:54 and 15:17:51, comprising 107460 samples per sensing location, being conventionally (i.e., uniformly) sampled at 200Hz. The considered dataset pertains to ambient wind and traffic dynamic loads that sufficiently excite the first few modes of the monitored bridge. These raw signals acquired by the tethered sensor network in Figure 11 are pre-processed as follows. Firstly, baseline adjustment is applied to the raw data to remove the mean value and any potential low-frequency trend within each acceleration response signal. Next, a 4th-order Butterworth band-pass filter is employed within the frequency range [0.15, 50] in Hz. For illustration, the left panel in Figure 12 plots the "corrected" signal (i.e., baseline

adjusted and band-pass filtered) obtained from the sensor #13. Further, its magnitude Fourier spectrum normalized to its peak value is plotted in the middle panel of Figure 12 for the frequency range [0, 20] Hz, within which the first four modes of the vibrating bridge lie[33]. Lastly, the right panel of Figure 12 plots the normalized magnitude Fourier coefficients sorted in descending order. On the last plot, a heuristically selected threshold at 5% of the peak Fourier spectrum magnitude (red broken line) is shown, indicating that the significant signal energy is captured from approximately 10000 Fourier coefficients. Thus, the actual sparsity level of the considered field recorded signals is roughly $K≈10000$. As previously discussed, though, no such information would be available from the low-rate data acquisition using the two sub-Nyquist spectral estimation approaches of Figure 1, but it is only reported to inform the comparison of the OMA results discussed in the following sub-section.
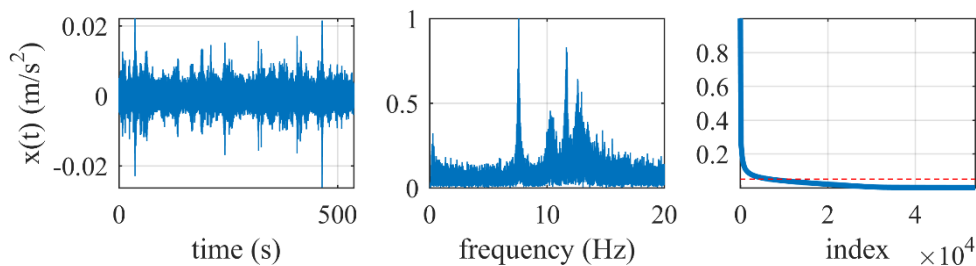

Figure 12: Typical acceleration response signal measured at sensor #13; (left panel): time history;(middle panel): Normalized Fourier spectrum magnitude within the frequency range of [0, 20] Hz; (right panel): Normalized magnitude Fourier coefficients in descending order. The red broken line signifies an arbitrary threshold at normalized Fourier spectrum of 0.05.

Given that the PSBS-based spectral estimation approach anticipates signal stationarity, the standard non-parametric Reverse Arrangement method **Error! Reference source not found.** is further applied on the considered acceleration response dataset to statistically test the stationarity hypothesis, which is confirmed at the 95% confidence level.

5.2 Mode shapes estimation of the Bärenbohlstrasse bridge

The same steps detailed in sub-sections 4.2 and 4.3 (see also Figure 1) are herein taken to estimate the mode shapes of the Bärenbohlstrasse bridge from the 18 corrected (i.e., baseline-adjusted and

band-pass filtered) field recorded acceleration responses. Table 2 collects the parameters adopted for the random CS-based and the deterministic multi-coset sampling at the same two *CRs* considered before (i.e., 31% and 11%). Table 2 also reports the sub-Nyquist sampling rates achieved by the adopted *CRs* based on the maximum cut-off frequency of the filtering operation at 50Hz, which pertains to an assumed Nyquist sampling rate at 100Hz.

Table 2: Considered parameters for the CS-based and the PSBS-based approaches for OMA of the structure in Figure 11 for two different compression ratios.

	Compression ratio	*CR*	**31%**	**11%**
Common parameters for both approaches	*Number of samples uniformly acquired in time*	N	107460	107460
	Sub-Nyquist Sampling Rate (Assumed Nyquist sampling rate at 100Hz)		**62.5%**	**21.9%**
	Number of Sub-Nyquist/Compressed samples	M	33581	11753
CS-based approach	*Target Sparsity Level*	K_T	1200-11160	1200-3840
PSBS-based approach	*Number of channels*	$\bar{M}$	5	14
	Down-sampling	$\bar{N}$	16	128
	Sampling pattern	**n**	$[0,1,2,5,8]^T$	$[0,1,2,6,8,20,29,38,47,50,53,60,63,64]^T$

Further, Table 2 presents the range of different K_T values (<M/3) considered in the CS-based approach, which are directly related to the algorithmic trade-off between accuracy and complexity. The latter reflects on the required running time of the CS signal reconstruction algorithm for various K_T values. As an example, Figure 13 plots the off-line computational time required by the CoSaMP algorithm to recover the 18 bridge acceleration responses from the acquired compressed measurements at *CR*=31% and 11% (left and right panel in Figure 13, respectively). From this figure, it is readily observed that the CS computational cost exponentially increases with K_T. For comparison, Figure 13 also depicts the running time of the PSBS-based approach (broken line) associated with the 18x18 spectral matrix estimation detailed in Eqs. (6) and (7). All reported numerical work was performed on a quadcore Intel Core i7-6700HD with 16GB RAM.
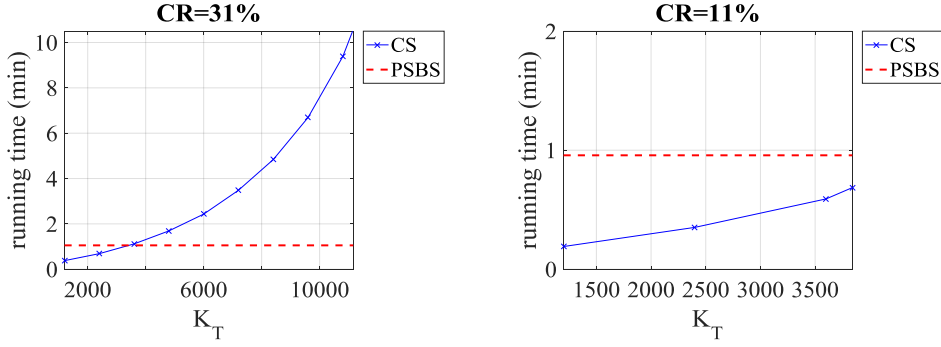
Figure 13: Total running time for off-line signal and power spectral recovery required by the CS-based and the PSBS-based approach, respectively, versus reconstruction sparsity level for CR=31% (left) and CR=11% (right)

As a final step, the standard FDD algorithm is applied to the PSD matrices estimated by the CS-based and the PSBS-based spectral estimation approaches reviewed in sections 2 and 3, respectively, to extract the bridge mode shapes. For illustration, Figure 14 plots the first four mode shapes of the considered bridge corresponding to two bending (modes 1 and 2) and two rotational (modes 3 and 4) vibrating modes. They are obtained from the standard FDD method using: (1) the 18 conventionally acquired signals, each comprising N=107460 samples (top panels); (2) the CS-based approach for CR=11% and K_T=3840; and (3) the PSBS-based approach for CR=11% (lower panels).

From a qualitative inspection of these mode shapes, it can be deduced that both the sub-Nyquist methods can adequately capture the shapes of the modal responses as estimated from the uniformly sampled dataset. However, non-negligible differences are observed between the conventional FDD and the CS-based approach, especially for the 2nd and the 4th vibrating modes.
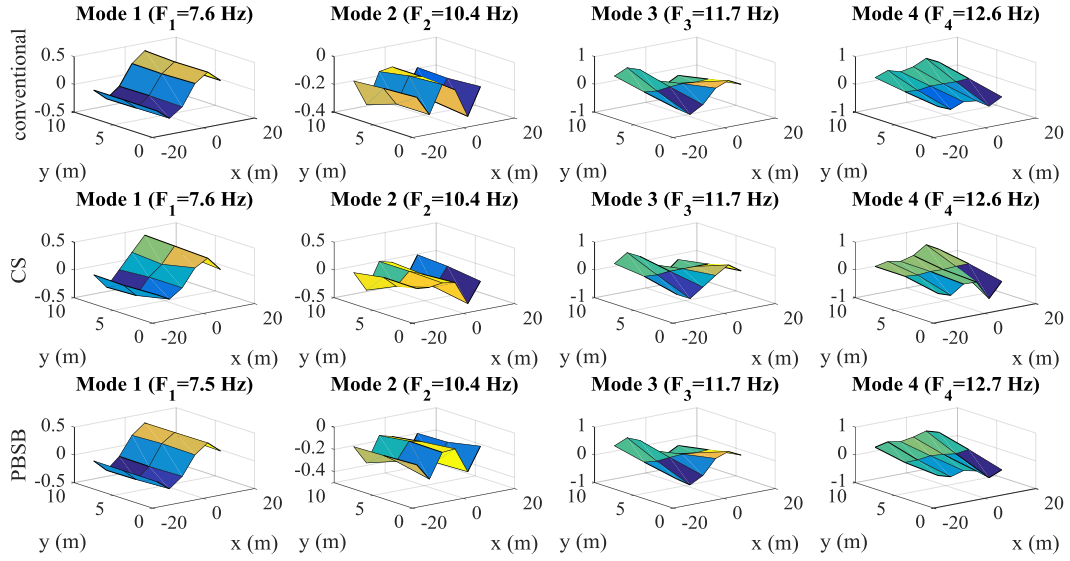
26

Figure 14: Mode shape estimation using: the conventional FDD (top); the CS-based approach for CR=11% and target reconstruction sparsity $K_T=3840$ (middle); the PSBS-based approach for CR=11% (bottom)

To quantify the level of similarity between mode shapes obtained from the conventionally sampled dataset and from the sub-Nyquist sampled acceleration responses, the MAC in Eq. (9) is plotted in Figure 15 and Figure 16 for the two considered *CR*s, respectively, as a function of the assumed target sparsity K_T for the CS-based (solid blue curve) and for the PSBS-based (red broken line) approaches.
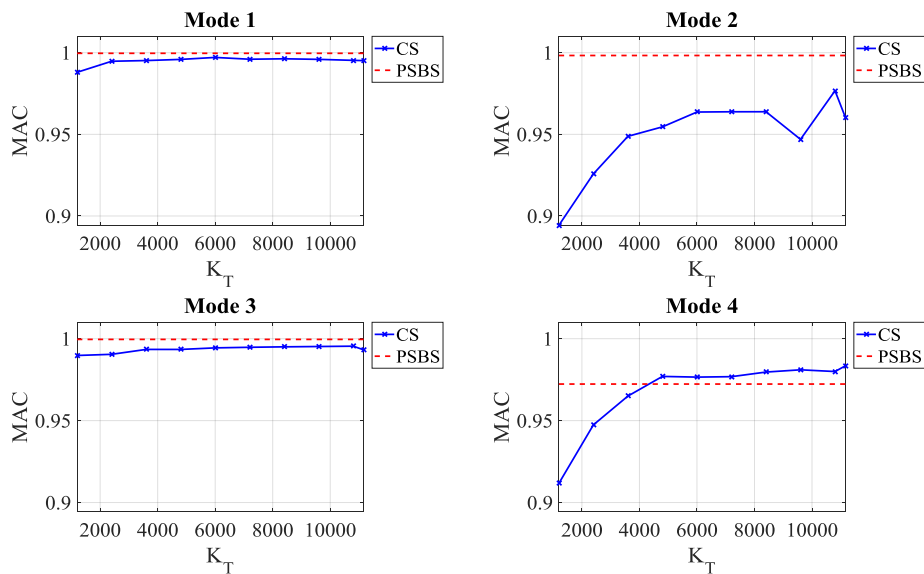

Figure 15: MAC versus reconstruction sparsity level K_T, obtained from the two considered approaches (i.e., PSBS-based and CS-based FDD) for CR= 31%
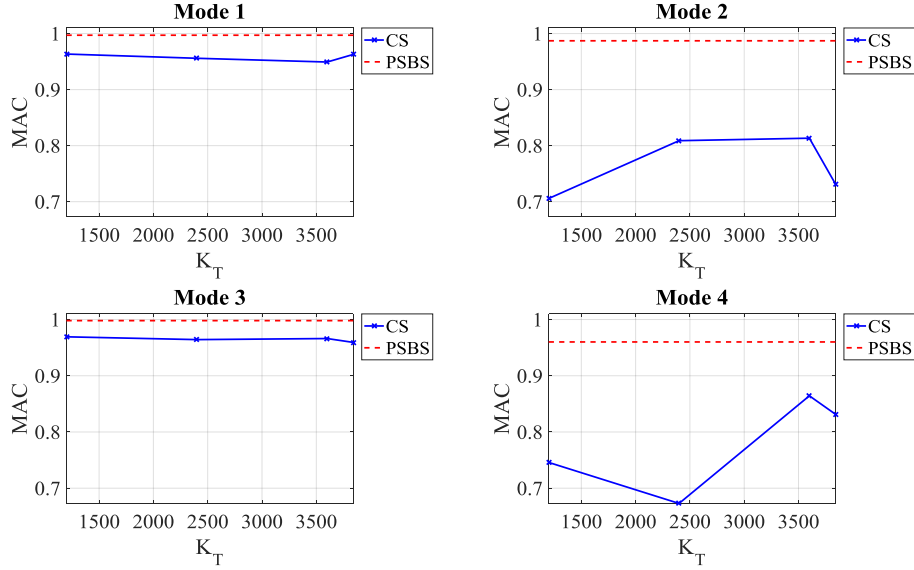
Figure 16: MAC versus reconstruction sparsity level KT, obtained from the two considered approaches (i.e., PSBS-based and CS-based FDD) for CR= 11%.

It is confirmed that the PSBS-based method outperforms in accuracy the CS-based approach, yielding higher MAC values in most of the cases considered. More importantly, the PSBS-based approach provides mode shapes exhibiting nearly unit MACs, even in the case of CR=11% (i.e., using almost 90% fewer measurements from the traditionally acquired signals) without the need to assume a target sparsity level. On the antipode, the CS-based approach is considerably affected by the assumed K_T values. In fact, for the smaller compression level considered (CR=31%), better accuracy is achieved for larger K_T values for all mode shapes, at the expense of higher computational cost during the sparse recovery step (see Figure 13). However, such monotonic trends of MAC with K_T are not confirmed for all the mode shapes for the case of CR=11% in Figure 16, while the 2nd and 4th modes are not satisfactorily estimated regardless of the K_T value (i.e., MAC values lying below 0.9 are commonly used as a practical criterion for rejecting mode shapes as inaccurate). As discussed before, this poor performance of the CS-based approach is related to the underlying level of sparsity of the acquired signals with respect to the number of compressed measurements, M, assumed. Specifically, based on the assumption that K=10000 for all signals considered in the dataset

(see the right panel of Figure 12), the number of compressed measurements that provides reasonably accurate signal recovery results should be in the order of $M \approx K \cdot \log(N) \approx$ 10000·log(107460) ≈50000 (see also *O'Connor et al.*[9,10]). In this respect, the unsatisfactory performance of the CS-based approach for *CR*=11% can be attributed to the fact that the number of compressed measurements (*M*=11753) randomly taken to achieve *CR*=11% is significantly lower from the above assumed $K \cdot \log(N)$ value, which, apparently, is not the case for *CR*=31% corresponding to about three time more measurements (*M*=33581). Remarkably, it appears that the performance of the PSBS approach in terms of MAC values is almost insensitive to *CR*. Nevertheless, it was deemed prudent not to consider lower *CR* values in this numerical assessment, since this would require a large number of cosets ($\bar{M} > 14$) or parallel channels in Figure 2 to satisfy the theoretical constraint of $\bar{M}^2 \geq \bar{N}$, as discussed in Section 3. In fact, one may note that even the consideration of $\bar{M} = 14$ channels may be unrealistic in practice. However, this is a setting that has been used before in pertinent theoretical studies[14,30,32], while recent advancements in the hardware implementation of multi-coset samplers provide *CR*s independently of the number of interleaved ADCs[37].

As a final remark, it is expected that the gains to the *CR* achieved by the PSBS approach compared to the CS-based approach in accomplishing quality OMA estimates, as those reported above, would reflect analogously to energy savings in WSNs[7,9]. This is because wireless data transmission is by far the most power-hungry operation in wireless sensors, being directly related to the amount of data, *M*, transmitted from each sensor in the considered setting. Further, higher gains in the overall energy-efficiency will be achieved for larger WSN deployments[9]. However, we refrain from reporting any particular estimate for the anticipated energy savings since these would depend on several parameters such as the WSN topology, the utilized wireless communication protocol, and the energy requirements of the multi-coset samplers. The latter is significantly influenced by the underlying technology used for multi-

coset sampling which is an open area of research in the sensors community and lies beyond the scope of this work.

6   CONCLUDING REMARKS

The performance of a CS-based approach vis-a-vis a PSBS-based approach for spectral estimation relying on sub-Nyquist random and deterministic multi-coset sampling schemes, respectively, has been numerically assessed in undertaking OMA. Both the approaches aim to reduce data transmission payloads facilitating reliable and cost-efficient long-term OMA via WSNs. This is accomplished by considering compressed structural acceleration responses acquired at sub-Nyquist rates and wirelessly transmitted to a base station without any local on-sensor data processing. The adopted approaches estimate the PSD matrix of the acceleration signals by operating directly to the sub-Nyquist/compressed measurements at the base station. Then, the standard FDD algorithm for OMA is applied to the estimated PSD matrix to extract structural mode shapes.

The quality of mode shapes obtained from structural response acceleration signals compressed at 31% and 11% below the Nyquist sampling rate (i.e., *CR*= 31% and 11%) using the two considered approaches have been quantified through the MAC with respect to mode shapes extracted from Nyquist sampled acceleration signals. For this purpose, two different sets of acceleration signals have been considered. The first set was generated through linear response history analysis applied to a white-noise excited finite element model of a simply supported steel beam. Additive white Gaussian noise was considered at *SNR*=10dB to produce a suite of relatively low-sparse acceleration signals in the frequency domain, aiming to gauge the influence of signal sparsity to the performance of the considered approaches vis-à-vis the high-sparse noiseless signals. The second dataset was acquired from an array of 18 tethered sensors deployed onto a particular overpass in Zurich, Switzerland open to the traffic. Pertinent post-processing and statistical stationarity tests were applied to the field recorded data prior to

compressive sampling.

It has been numerically shown and theoretically justified, that, for a given sub-Nyquist sampling rate, the capability of the CS-based approach to extract faithful estimates of the mode shapes depends heavily on the target sparsity level, K_T, which needs to be assumed in the CS signal reconstruction step. It has also been demonstrated that the accuracy of the CS-based approach improves at larger K_T values at the cost of higher computational effort reflected on the increased required runtime of the adopted CS sparse signal recovery algorithm. However, no increase to the assumed K_T value can compensate for the acquisition of an excessively small number of compressed measurements which is the case for CR=11% for all the sets of acceleration signals considered in this work. In this regard, it is concluded that conservative compression ratios should be adopted in using the CS-based approach to ensure acceptable quality of modes shapes, especially in the case where no prior knowledge on the acceleration signal sparsity is available.

On the antipode, it was numerically shown that the PSBS-based approach, which treats response acceleration signals as wide-sense stationary stochastic processes without imposing any signal sparsity conditions, performs equally well and consistently better than the CS-based approach in extracting mode shapes for all the herein considered sets of compressively sampled acceleration signals. In fact, the PSBS-based approach yields MAC>0.96 even for the low-sparse signals contaminated with white noise at SNR=10dB and for low sampling rates at CR=11% (i.e., 89% below the Nyquist rate).

Overall, the herein furnished numerical data demonstrate that the inherent signal agnostic attributes of the PSBS-based approach renders this method more advantageous compared to the CS-based approach in OMA applications where high signal compression levels are desired to address sensor power consumption and wireless bandwidth transmission limitations. Further, the developed PSBS approach retrieves only the signals second order statistics (i.e., covariance

31

and power spectral estimates) and extracts structural modal properties directly from the acquired compressed data yielding computationally efficient OMA. It is recognized, though, that the PSBS approach is strictly a spectral estimation method that does not return the monitored signals deterministically in time domain. This limits the use of PSBS to structural health monitoring applications where time-domain signal monitoring is not of essence as in the case of frequency domain based OMA. Still, further research is warranted to assess the potential of the considered PSBS-based spectral estimation approach in actual field deployments. Such an assessment necessitates the development of custom-made wireless sensors featuring either multi-coset samplers at the hardware level or, alternatively, efficient algorithms for off-line on-sensor multi-coset sampling. These aspects are left for future work by the authors.

AKNOWLEDGEMENTS

REFERENCES

1. Reynders E. System Identification Methods for (Operational) Modal Analysis: Review and Comparison. *Arch Comput Methods Eng* 2012; 19(1): 51–124.

2. Brincker R, Ventura CE. *Introduction to Operational Modal Analysis*. Chichester, UK: John Wiley & Sons, 2015.

3. Lynch JP. An overview of wireless structural health monitoring for civil structures. *Philos Trans R Soc A Math Phys Eng Sci* 2007; 365(1851): 345–372.

4. Lynch JP, Loh KJ. A Summary Review of Wireless Sensors and Sensor Networks for Structural Health Monitoring. *Shock Vib Dig* 2006; 38(2): 91–128.

5. Nagayama T, Spencer BFJ. Structural health monitoring using smart sensors. *Report No NSEL-001 Newmark Structural Engineering Laboratory University of Illinois at Urbana-Champaign* 2007.

6. Spencer BF, Yun C. Wireless Sensor Advances and Applications for Civil Infrastructure Monitoring. *Report No NSEL-024 Newmark Structural Engineering Laboratory University of Illinois at Urbana-Champaign* 2010.

7. Lynch JP, Sundararajan A, Law KH, Kiremidjian AS, Carryer E. Power-efficient data management for a wireless structural monitoring system. In*: 4th Int Work Struct Heal Monit*, Stanford, CA 2003; 1177–1184.

8. Bao Y, Beck JL, Li H. Compressive sampling for accelerometer signals in structural health monitoring. *Struct Heal Monit* 2011; 10(3): 235–246.

9. O'Connor SM, Lynch JP, Gilbert AC. Compressed sensing embedded in an operational wireless sensor network to achieve energy efficiency in long-term monitoring applications. *Smart Mater Struct* 2014; 23(8): 085014.

10. O'Connor SM, Lynch JP, Gilbert AC. Implementation of a compressive sampling scheme for wireless sensors to achieve energy efficiency in a structural health monitoring system. In: Yu TY, Gyekenyesi AL, Shull PJ, et al. (eds) *Proceedings of SPIE - The International Society for Optical Engineering*. San Diego, CA, USA 2013; 86941L.

11. Klis R, Chatzi E. Data recovery via Hybrid Sensor Networks for Vibration Monitoring of Civil Structures. *Int J Sustain Mater Struct Syst* 2015; 2(1/2): 161-184.

12. Yang Y, Nagarajaiah S. Output-only modal identification by compressed sensing: Non-uniform low-rate random sampling. *Mech Syst Signal Process* 2015; 56–57: 15–34.

13. Park JY., Wakin MB., Gilbert AC. Modal analysis with compressive measurements. *IEEE Trans Signal Process* 2014; 62(7): 1655–1670.

14. Gkoktsi K, Giaralis A, TauSiesakul B. Sub-Nyquist signal-reconstruction-free operational modal analysis and damage detection in the presence of noise. In: Lynch JP (ed) *SPIE Smart Structures and Materials + Nondestructive Evaluation and Health Monitoring,* Las Vegas, NV, 2016.

15. Duarte MF, Shen G, Ortega A, et al. Signal compression in wireless sensor networks. *Philos Trans A Math Phys Eng Sci* 2012; 370(1958): 118–135.

16. Donoho DL. Compressed sensing. *IEEE Trans Inf Theory* 2006; 52(4): 1289–1306.

17. Candès EJ, Romberg J, Tao T. Robust uncertainty principles: Exact signal reconstruction from highly incomplete frequency information. *IEEE Trans Inf Theory* 2006; 52(2): 489–509.

18. Baraniuk R. Compressive Sensing [Lecture Notes]. *IEEE Signal Process Mag* 2007; 24(4): 118–121.

19. Needell D, Tropp JA. CoSaMP: Iterative signal recovery from incomplete and inaccurate samples. *Appl Comput Harmon Anal* 2009; 26(3): 301–321.

20. Marple SL. *Digital Spectral Analysis with Applications*. Englewood Cliffs, New Jersey: PTR Prentice Hall,1987.

21. Bao Y, Li H, Sun X, Yu Y, Ou J. Compressive sampling-based data loss recovery for wireless sensor networks used in civil structural health monitoring. *Struct Heal Monit* 2013; 12: 78–95.

22. Zou Z, Bao Y, Li H, Spencer B, Ou J. Embedding compressive sensing-based data loss recovery algorithm into wireless smart sensors for structural health monitoring. *IEEE Sensors Journal* 2015; 15, 797–808.

23. Huang Y, Beck JL, Wu S, Li H. Bayesian compressive sensing for approximately sparse signals and application to structural health monitoring signals for data loss recovery. *Prob Eng Mech* 2016; 46: 62-79.

24. Klis R, Chatzi EN. Vibration monitoring via spectro-temporal compressive sensing for wireless sensor networks. *Struct Infrastruct Eng* 2017; 13(1): 195–209.

25. Davenport MA, Laska JN, Treichler JR, et al. The Pros and Cons of Compressive Sensing for Wideband Signal Acquisition: Noise Folding versus Dynamic Range. *IEEE Trans Signal Process* 2012; 60(9): 4628–4642.

26. Axell E, Leus G, Larsson E, et al. Spectrum Sensing for Cognitive Radio : State-of-the-Art and Recent Advances. *IEEE Signal Process Mag* 2012; 29(3): 101–116.

27. Duarte MF, Baraniuk RG. Spectral compressive sensing. *Appl Comput Harmon Anal* 2013; 35(1): 111–129.

28. Davenport MA, Wakin MB. Compressive sensing of analog signals using Discrete Prolate Spheroidal Sequences. *Appl Comput Harmon Anal* 2012; 33(3): 438–472.

29. Venkataramani R, Bresler Y. Optimal sub-nyquist nonuniform sampling and reconstruction for multiband signals. *IEEE Trans Signal Process* 2001; 49(10): 2301–2313.

30. Ariananda DD, Leus G. Compressive Wideband Power Spectrum Estimation. *Signal Process IEEE Trans* 2012; 60(9): 4775–4789.

31. Jingchao Z, Peizhuo L, Ning F, et al. Prototype design of multicoset sampling based on compressed sensing. In: *2015 IEEE 12th International Conference on Electronic Measurement & Instruments (ICEMI'2015)*. Qingdao, Shandong, China, 2015; 1303–1308.

32. Tausiesakul B, Gonzalez-Prelcic N. Power Spectrum Blind Sampling Using Minimum Mean Square Error and Weighted Least Squares. In: *47th Asilomar Conference Signals, Systems and Computers (ACSSC)* 2013; 153–157.

33. Spiridonakos MD, Chatzi EN, Sudret B. Polynomial Chaos Expansion Models for the Monitoring of Structures under Operational Variability. *ASCE-ASME J Risk Uncertain Eng Syst Part A Civ Eng* 2016; 2(3): B4016003.

34. Chatzi EN, Spiridonakos MD. Incorporating Uncertainty in Vibration-Based Monitoring and Simulation. In: *Fourth International Conference on Soft Computing Technology in Civil, Structural and Environmental Engineering (CIVIL-SOFT-COMP 2015)*. Prague, Czech Republic, 2015.

35. Candès EJ. The restricted isometry property and its implications for compressed sensing. *Comptes Rendus Math* 2008; 346(9-10): 589–592.

36. Vaswani N, Zhan J. Recursive Recovery of Sparse Signal Sequences from Compressive Measurements: A Review. IEEE Trans Signal Process 2016; 64(13): 3523–3549.

37. Moon T, Choi HW, Tzou N, Chatterjee A. Wideband Sparse Signal Acquisition with

Dual-rate Time-Interleaved Undersampling Hardware and Multicoset Signal Reconstruction Algorithms. *IEEE Trans Signal Process* 2015; 63(24): 6486–6497.

38. Ji X, Hikino T, Kasai K,Nakashima M. Damping identification of a full-scale passively controlled fine-story steel building structure. *Earthquake Eng Struct Dyn* 2013; 42(2): 277-295.